CARBON 89 (2015) 188–196

Available at www.sciencedirect.com
ScienceDirect
journal homepage: www.elsevier.com/locate/carbon

Observation of different charge transport regimes and large magnetoresistance in graphene oxide layers

A. Vianelli [a,b,*], A. Candini [b], E. Treossi [c], V. Palermo [c], M. Affronte [a,b]

[a] Dipartimento di Scienze Fisiche, Informatiche e Matematiche, Università di Modena e Reggio Emilia, Via G. Campi 213/a, 41125 Modena, Italy
[b] Centro S3, Istituto Nanoscienze – CNR, Via G. Campi 213/a, 41125 Modena, Italy
[c] ISOF – Istituto per la Sintesi Organica e la Fotoreattività, CNR Area della Ricerca di Bologna, Via P. Gobetti 101, 40129 Bologna, Italy

ARTICLE INFO

Article history:
Received 21 October 2014
Accepted 6 March 2015
Available online 13 March 2015

ABSTRACT

We report a systematic study on charge transport properties of thermally reduced graphene oxide (rGO) layers, from room temperature to 2 K and in presence of magnetic fields up to 7 T. The most conductive rGO sheets follow different transport regimes: at room temperature they show an Arrhenius-like behavior. At lower temperature they exhibits a thermally activated behavior with resistance R following a $R = R_0\exp(T_0/T)^p$ law with $p = 1/3$, consistently with 2D Mott Variable Range Hopping (VRH) transport mechanism. Below a given temperature T_c, we observe a crossover from VHR to another regime, probably due to a shortening of the characteristic lengths of the disordered 2D system. The temperature T_c depends on the reduction grade of the rGO. Magnetoresistance $\Delta R/R$ of our rGO films shows as well a crossover between positive and negative and below liquid He temperature $\Delta R/R$ reaches values larger than ~–60%, surprisingly high for a – nominally – non magnetic material.

1. Introduction

Graphene oxide (GO) has a history much older and complex than the one of graphene [1,2]: the first well-known study was published back in 1859 by Brodie [3], who was studying the structure and the molecular weight of graphite. A renewed interest around GO spread after 2004 as promising viable route to obtain large area, processable monoatomic sheets. Differently from pristine graphene, GO shall be obtained with sheets size tunable from >100 μm to <1 μm [4], can be functionalized with different molecular moieties [5] allowing to process it in water or organic solvents [6] and to deposit it on different substrates with a very high monolayer yield [7]. Alongside, the low cost of production, the high solubility and wide processability, the optical transparency, the tunability of electrical and optical properties of GO and the possibility of chemical functionalization, makes it suitable for many applications, such as production of paper-like material [8], conductive electrode for flexible electronics [7,9], energy storage [10–15], optical applications [16] and gas sensing [17–19] among others. Reduced graphene oxide (rGO) has high potential applications, in some fields even

* *Corresponding author at:* Dipartimento di Scienze Fisiche, Informatiche e Matematiche, Università di Modena e Reggio Emilia, Via G. Campi 213/a, 41125 Modena, Italy.
E-mail address: anna.vianelli@unimore.it (A. Vianelli).
http://dx.doi.org/10.1016/j.carbon.2015.03.019
0008-6223/

better than graphene: rGO-based highly porous, conductive substrates for supercapacitors can reach surface areas >3100 m^2/g and capacitance ~150 F/g; in batteries, it can act as a scaffold for lithium-storing materials [12]; in sensors, Nokia researchers have recently demonstrated GO-based humidity sensors with performance better than commercial state-of-the-art [18].

All these applications will rely on understanding and tuning the mechanisms of charge transport in rGO. However, the structure and electrical properties of rGO are much more difficult to model than the ones of graphene, due to the disordered structure of rGO, which is not uniform on the 1–10 nm scale, and depends strongly on the preparation and reduction processes used to produce rGO [20].

Generally speaking, GO can be seen as a graphene-like structure where different functional groups such as carboxyl, carbonyl, hydroxyl and epoxy decorate the surface, giving rise to a variable sp^2 and sp^3 hybridized carbon ratio. Due to its nonstoichiometric atomic composition and to its amorphous nature, there are different structural model for the GO [21], which are still under debate. The prevailing one, the Lerf–Klinowski (LK) model [22], predicts GO to be composed by two different domains that are randomly distributed: intact graphene domains, with sp^2-hybridized carbon atoms and oxidized domains, which are sp^3-hybridized due to the presence of the aforementioned functional groups. These domains destroy the long-range conductivity interrupting the conjugation of the graphene-like domains, making GO an electrical insulator.

The reduction of GO, i.e. the removal of the oxygen-containing functional groups, partially restores the sp^2 conjugated network allowing the creation of percolating pathways between the intact graphene-like domains, and the material is transformed from an insulator into a graphene-like semimetal [23], although several defects remain anyhow in the final graphene lattice.

The reduction of GO can be achieved either via thermal annealing [24,25], chemical treatments [26] or electrochemical processes [13,27–30]. Chemical or electrochemical reduction are the most widely used because can be performed in liquids, producing large amount of rGO with cheap and easy techniques. The drawback is that harmful chemicals are frequently involved, moreover the effect of a specific reagent is selective, preventing the elimination of all the oxygen-containing functional groups. Thermal mediated reduction instead, is more effective and thanks to high temperatures can heal the structural defects through graphitization. On the other hand it has been proved that rapid increase of temperature provokes the release of CO and CO_2 gases at high pressure [21,23], which damages the structure and creates morphological defects. An interplay of these two processes occurs, limiting the final efficiency of thermal annealing.

All these methods lead to a final rGO with varying degrees of reduction in terms of electrical and morphological properties.

Despite a huge number of publications focus on applications of GO in diverse fields, a full control of charge transport has not been achieved and more systematic studies could widen the GO potentials for electronic applications.

Usually the electric transport in reduced graphene oxide is described within a variable range hopping model. From the paper of Gomez-Navarro et al. [31] who first suggested Mott Variable Range Hopping (VRH) as the dominant charge transport mechanism down to around 80 K in individual chemically reduced GO flakes, a number of other groups reported similar results [32–35]. Deviations from Mott-VHR model are observed at high temperatures, ascribed to a crossover to an Arrhenius-like regime [33], while electric-field-driven tunneling has been proposed as the dominant mechanism at very low temperatures and high electric fields [32]. Wang et al. [36], found that transport is governed by two different Arrhenius equations in the high- and low-temperature regime, while Joung and Khondaker [37] proposed 2D Efros-Shklovskii VRH as dominant transport mechanism in their rGO films. All these studies were limited in temperature and in the level of GO reduction, thus a fragmented scenario appears from this literature.

Another interesting scientific challenge is to understand the magnetic properties of GO. Only few papers study the electrical transport of rGO under an applied magnetic field. Zhou et al. [38] reported a change from positive to negative magnetoresistance in pristine graphene where artificial disorder was introduced gradually. In very disordered samples they observe a significant non-saturating negative magnetoresistance up to several percents. Wang et al. [36] and Muchharla et al. [35] reported negative magnetoresistance of much lower intensities in chemically reduced graphene films.

Herein we present a systematic study of the electrical properties of thermally reduced GO films, which were prepared at several reduction levels in a controllable way, i.e. by changing the annealing temperature. It has been possible to achieve distinct resistive states of rGO, which allow us to control rGO electrical characteristics through a simple fabrication protocol. We also report the magnetic field dependence of the resistance, finding a non-saturating negative magnetoresistance exceeding 60% at 2 K.

2. Experimental details

2.1. *Samples preparation and characterization*

Graphene oxide was prepared by a modified Hummers method, following a procedure described in previous work [4]. Graphene oxide powders obtained in this way were dispersed in water by sonication and purified by dialysis. Larger aggregates were removed by centrifugation at 14,000 rpm before processing. The resulting lateral dimension of the sheets is of the order of 1–2 μm (see Supplementary contents and for a more detailed analysis Ref. [39]).

GO was deposited on a commercially available silicon wafer with nominally 300 nm of silicon dioxide insulating layer by spin coating. The film thickness is ~10 nm for all our devices. The wafer was plasma cleaned before the deposition using oxygen as gas, in order to clean the surface and make it hydrophilic. Typical lateral dimensions of our samples are 0.8 × 3 mm (for more details see Supplementary contents).

Reduction of GO was obtained by thermal annealing. The samples were treated in high vacuum (10^{-6} mbar) to avoid material losses. Heat treatments were carried out at 200 °C, 300 °C, 500 °C, 600 °C, 700 °C and 940 °C for 1 h (see Supplementary contents for more details). We denote samples annealed at these temperatures as sample A, B, C, D, E and F, respectively. After the heat treatment, samples were kept in vacuum out of the furnace while they cooled down naturally. Electrical contacts were provided after the annealing by thermal evaporation of two rectangular gold contacts of 100 nm thickness in a high vacuum chamber (10^{-6} mbar). In order to improve the adhesion between gold and silicon dioxide a thin layer of chrome (10 nm) was evaporated before gold in the same chamber.

To investigate the characteristics of the deposited GO films, we used both AFM imaging and micro Raman spectroscopy (632.81 nm excitation). The AFM analysis shows that the average roughness of the film is 2.7 nm in agreement with Ref. [40] (see Supplementary contents). The height profile across the film border shows a thickness of ~10 nm (Fig. 1a).

Micro-Raman measurements show the typical features of graphene oxide [41–43]: the G-peak at ~1580 cm^{-1}, usually assigned to in-phase vibration of the graphite lattice, and the D-peak at ~1350 cm^{-1} which is assigned to local defects and disorder especially at the edges of graphene and graphite platelets (Fig. 1b).

2.2. Measurements details

Resistance measurements were carried out in a Quantum Design Physical Properties Measurements System (PPMS) by using an external Keithley 2636 Source-Meter. *I*–*V* characteristics were systematically measured to check the ohmic character of the signal. Then, current measurements were taken at a fixed reading voltage of 100 mV or 200 mV while sweeping the temperature (between 2 and 300 K) or the magnetic field (up to 7 T applied either perpendicular or parallel to the film surface in positive and negative orientations). The sample resistance was measured in two- or four-probe configuration without finding any substantial differences (see Supplementary contents).

3. Results

3.1. Control of room temperature resistivity

Before the reduction, the resistance of the samples is above the instrumentation limits, confirming the insulating nature of the pristine GO. After the annealing, the *I*–*V* characteristics become linear in the range of ±500 mV, indicating that ohmic conduction was activated for all the heat treatments we have done (see Supplementary contents). Even for heat treatment at temperature as low as 200 °C, the resistor acquired a certain electrical conductivity suggesting that reduction of GO is already activated at this temperature. From the linear *I*–*V* curves we extracted the room temperature (RT) resistivity ρ_{RT}, which could be tuned by more than 2 orders of magnitude by changing the annealing temperature (Fig. 2). ρ_{RT} for sample A is ~0.037 Ω m while for sample F is ~1.02×10^{-4} Ω m.

The increase of the annealing temperature (T_A) results in a decrease of the room temperature resistivity of the samples, which reflects a higher level of reduction of our GO. ρ_{RT} drops very fast by increasing T_A up to 700 °C, then it saturates for higher T_A. It is likely, that even though the graphene oxide is more reduced, and thus the sp^2 conjugated network is better restored, the transport is limited by the increase of topological defects and structural disorder introduced by the high temperature of the treatment.

This prevents GO to fully recover the electronic properties of pristine graphene [20,31,44]. Jung et al. [37] reported similar results of rGO resistance as a function of sp^2 carbon fraction.

After the annealing we performed micro-Raman spectroscopy to investigate the structural changes in the reduced graphene oxide films. The intensity of the D peak increases over the G peak as the reduction progresses with increasing annealing temperature, in agreement with previous reports [26,43,45–47] (see Supplementary contents). The I_D/I_G ratio is related to the sp^2 domain size through the empirical Tuinstra–Koenig relation [48], and thus the increase of the ratio can be explained as the creation of a high number of new graphitic domains smaller in size of the ones present in the GO before reduction. We point out, however, that I_D/I_G ratio measured before reduction presents an important

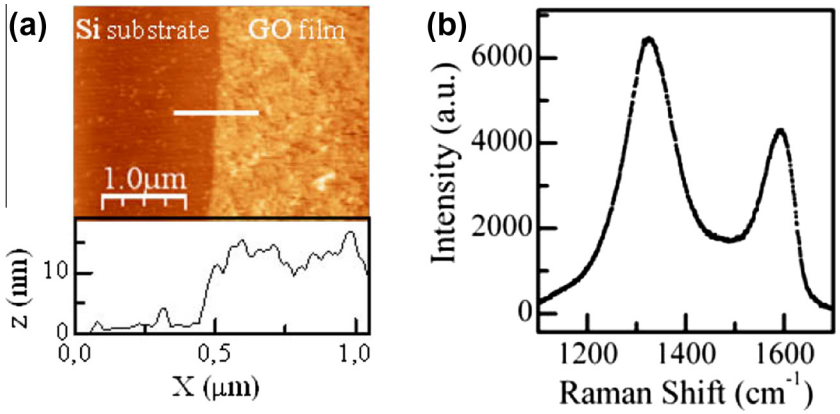

Fig. 1 – (a) AFM image of 10 nm thick GO film deposited on Si/SiO_2 substrate and below AFM section profile along the white line revealing the film thickness. (b) Micro-Raman spectrum of GO film before the thermal annealing, recorded at λ_{exc} = 632.81 nm. (A color version of this figure can be viewed online.)

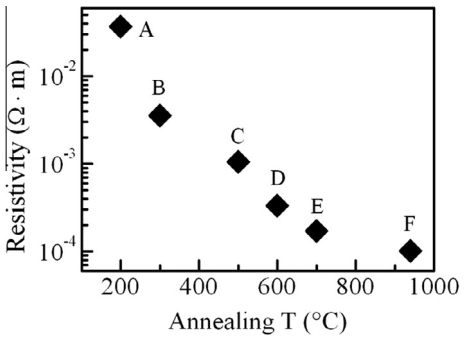

Fig. 2 – Room temperature resistivity of the rGO films as a function of the annealing temperature.

dispersion, which – we believe – makes the Raman analysis not sufficiently accurate to reveal the morphology of the rGO film. The reader can refer to other previously published studies for the relation between annealing temperature and final C/O ratio and sp^2 C–C content of the reduced graphene oxide, extracted from XPS data [25,37,49,50].

3.2. *Temperature dependence of the rGO resistivity*

In order to study the transport mechanisms in the rGO films, we measured the resistance (R) as a function of the temperature (T), from room temperature down to 2 K. The $R(T)$ curve may increase up to 5 orders of magnitude upon cooling. Samples A, B, C and D become too resistive to be measured down to 2 K, so their $R(T)$ curves span a smaller temperature range. We observe that the slope of resistivity increases faster by decreasing the degree of reduction of our GO.

For a generic thermally activated charge transport, $R(T)$ can be expressed as:

$$R = R_0 \exp{(T_0/T)^p}$$

where T_0 is the characteristic temperature of the activation process. In the case of hopping mechanism, p is the exponent which discriminates between different mechanisms and it is equal to $p = 1/(D + 1)$, with D being the dimensionality of the system [51]. In particular, the exponent p results to be equal to 1/3 for 2D Mott-VRH, 1/4 for 3D Mott-VRH, 1/2 for 2D Efros-Shklovskii VRH or 1 for thermally activated Arrhenius-like transport mechanism.

The behavior of the resistivity was analyzed by plotting the natural logarithm of ρ as a function of the four different power laws accounting for different temperature dependencies. In Fig. 3 we show an example of the comparison between the different transport models for sample E.

As evident in Fig3 we cannot find a single regime that extends in the whole temperature range we have studied, but this is not surprising, since disordered materials quite often exhibit more than one $\rho(T)$ law in such a broad T-range. Yet we can recognize that specific $\rho(T)$ dependencies appear systematically in all the reduced GO samples resistivity curves with a progressive extension of the interested temperature interval. In particular, taking into account all the different curves for all the samples (not shown), we find that the $R = R_0\exp(T_0/T)^{1/3}$ law spans the largest temperature range in all our samples: down to around 50 K, we actually find that

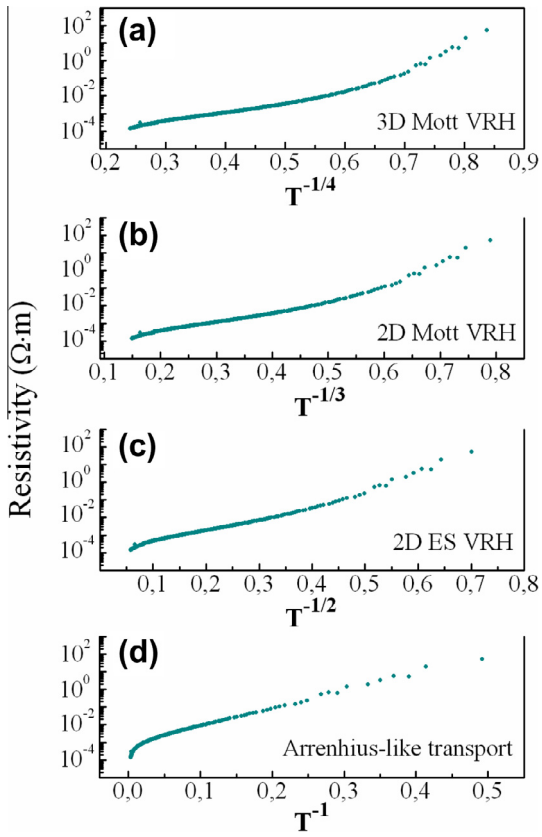

Fig. 3 – Comparison between the different transport model: log(ρ) as a function of T^{-x}, x being equal to (a) $x = 1/4$ for 3D Mott VRH, (b) $x = 1/3$ for 2D Mott VRH, (c) $x = 1/2$ for 2D ES VRH, and (d) $x = 1$ for the Arrhenius-like transport, for sample E. (A color version of this figure can be viewed online.)

experimental data of all our samples fit well the with 2D Mott VRH model.

To show that the $R = R_0\exp(T_0/T)^{1/3}$ is probably the most representative law for our set of data, we plot the resistivity in a semi-log plot as a function of $T^{-1/3}$ (Fig. 4a). Interestingly, the slopes of the linear fits scale with the degree of reduction of our GO. Within the framework of the Mott-VRH model, the characteristic temperature T_0 of the $R = R_0\exp(T_0/T)^{1/3}$ equation is given by:

$$T_0 = (3/k_B N(E_F)\xi^2)$$

where $N(E_F)$ is the DOS near the Fermi energy and ξ is the localization length. The values of T_0 extracted from the fits scales down with increasing T_A (Fig. 4b). Considering characteristic values of $N(E_F)$ ranging between 10^{14} and 10^{16} cm^{-2} eV^{-1} with increasing grade of reduction of the GO, we obtain localization length ξ ranging between 1.2 nm and 4.1 nm, which are typical sizes of graphitic domains in rGO [20,24,37,52]. The R_0 values span from 3×10^{-3} to 14×10^{-3} Ω (see Table 1 and Supplementary contents).

While for samples A and B ($T_A = 200$ and 300 °C, respectively) experimental data fit the $R = R_0\exp(T_0/T)^{1/3}$ law in the whole temperature range (down to 22 K for sample B), for more reduced GO, we observe deviations that occur at a

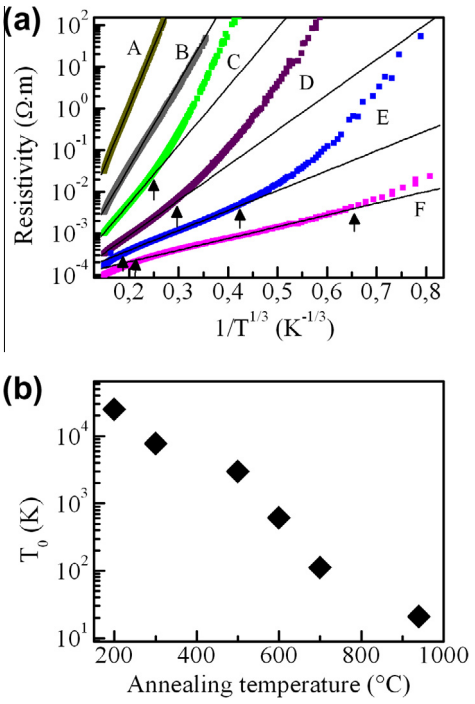

Fig. 4 – (a) Resistivity vs $1/T^{1/3}$ for different values of annealing temperature. Black arrows indicate the temperature at which a crossover from 2D-Mott VHR (black lines) to another activated regime takes places. (b) Characteristic temperature T_0 extracted from the $R = R_0\exp(T_0/T)^{1/3}$ fit. (A color version of this figure can be viewed online.)

Table 1 – Summary of room temperature resistance (R_{RT}), room temperature resistivity ρ_{RT} and characteristic temperature T_0 extracted from $R = R_0\exp(T_0/T)^{1/3}$ fit as a function of annealing temperature T_A.

Sample	T_A (°C)	R_{RT} (k Ω)	ρ_{RT} (Ω m)	T_0 (K)
A	200	656.4	3.67×10^{-2}	24,226
B	300	114.5	3.54×10^{-3}	8476
C	500	40.5	1.06×10^{-3}	2767
D	600	10.9	3.34×10^{-4}	604
E	700	3.4	1.71×10^{-4}	109
F	940	1.7	1.02×10^{-4}	22

crossover temperature T_c (marked by black arrows in Fig. 4a) which scales with the degree of reduction, going from 64 K for sample C (T_A = 500 °C) to 3.6 K for the sample F (T_A = 940 °C).

The $R = R_0\exp(T_0/T)^{1/3}$ behavior reflects the 2D dimensionality of the structure of the sheets. It has been proposed [24,52,53] that reduction of GO produces islands of intact graphene separated by clusters of point defects within a graphene flake. Hopping presumably occurs between the intact graphene regions by consecutive inelastic tunneling processes. The scaling of the slope of the $R(T)$ curves with increasing annealing temperature, clearly indicates a gain in the electrical conductivity due to a decrease of defect density and restoration of π–π bonds. Below the temperature T_c, a change of the electrical transport regime likely occurs. For disordered systems it is in fact possible to see crossovers between different regimes by lowering the temperature, due to the fact that the system's characteristic lengths change. However, from our data it is not possible to pinpoint the actual transport regime below T_c: the investigated temperature range is indeed too short to allow a clear discrimination.

For samples E and F (T_A = 700 °C and 940 °C, respectively) we also observe a crossover (at T = 153 K and T = 103 K, respectively) to a different regime characterized by a $R(T)$:

$$R = R_0\exp(E_g/k_BT)$$

where E_g is the activation energy and k_B is the Boltzmann constant (Fig. 5).

This is characteristic of an Arrhenius-like behavior [33] where 3D thermally activated processes start to dominate the conduction. Data fitting with $R = R_0\exp(E_g/k_BT)$ law gives activation energies of 26.5 meV and 11.7 meV for sample E and F, respectively, which are in good agreement with previously reported values [32,33,35].

The crossover from the 2D Mott-VRH to thermally activated regime is probably due to a increase of the characteristic lengths of the disordered 2D system and the beginning of a 3D conduction of charge carriers through the rGO film.

3.3. *Magnetoresistance measurements*

We have also studied the dependence of the resistance on an external magnetic field B applied perpendicular to the plane of the GO film. Samples A, B, and C turned out to be too resistive and the magnetoresistance $\Delta R/R = [R(B) - R(B = 0)]/R(B = 0)$, if any, is found to be within the electrical noise; therefore, we report magnetoresistance data only for samples D, E and F (T_A = 600 °C, 700 °C and 940 °C, respectively).

For all of our samples we find a room temperature negative magnetoresistance (see Fig. 4a). However, while sample F shows negative magnetoresistance down to the lowest temperature, for sample D and sample E we observe a change to positive magnetoresistance at a temperature that is comparable to the one where a crossover in $\rho(T)$ was observed (see Supplementary contents). Negative magnetoresistance in rGO samples have been also reported in Ref. [35,36,54] while the change of sign is probably related to the crossover

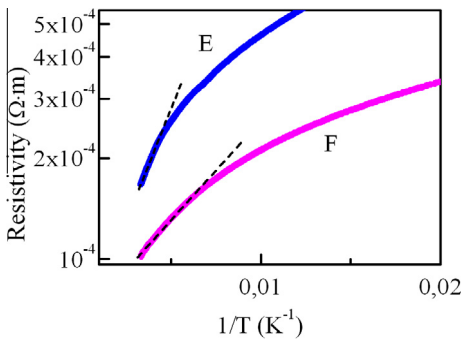

Fig. 5 – Arrhenius plot of resistivity for sample E and F. (A color version of this figure can be viewed online.)

between different regimes of charge transport as previously discussed.

The magnetoresistance intensity strongly depends on temperature. Fig. 6a shows the $\Delta R/R$ as a function of the applied magnetic field for sample F (T_A = 940 °C) at temperatures down to 2 K. The magnetoresistance of the rGO film does not show any saturation up to 7 T and the intensity reaches $\Delta R/R = -64\%$ at 2 K and 7 T in sample F, which is a surprisingly high value for a – nominally – non magnetic material.

Possible sources of the negative magnetoresistance are weak localization, dominance of (bi-)polaronic mechanism [55,56] and scattering from localized magnetic moments originated from vacancies and impurities [35]. The contribution of the negative magnetoresistance due to weak localization and (bi-)polaronic mechanism is expected to saturate at relative low magnetic fields (<1 T) and it should vanish for temperatures above 100 K [38].

This is not the case in our measurements, thus weak localization processes can be ruled out and contribution due to the scattering with the localized magnetic moments originated from disorder, defects and impurities should be considered as main source of high and negative magnetoresistance [35].

There is a lively literature about the influence of defects such as adatoms or vacancies on the magnetic properties of graphene-like materials. After this effect was predicted

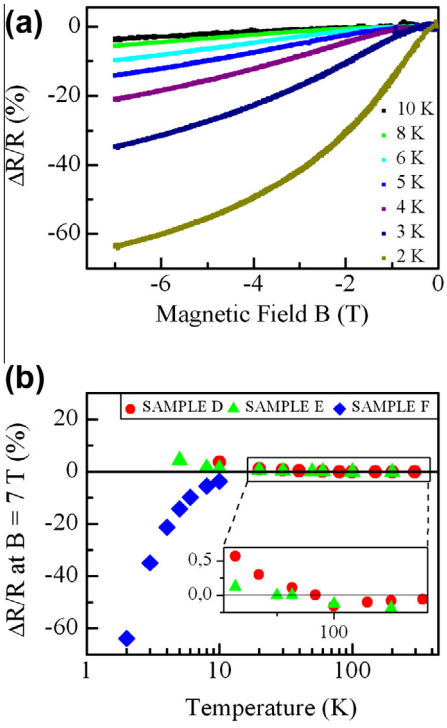

Fig. 6 – (a) Magnetoresistance of sample F at different temperatures and (b) the intensity of magnetoresistance at B = 7 T for sample D, E and F as a function of temperature. For sample D and sample E we see a crossover from negative to positive magnetoresistance lowering the temperature (Inset: zoom in on the interested region), while for sample F, the magnetoresistance is always negative. (A color version of this figure can be viewed online.)

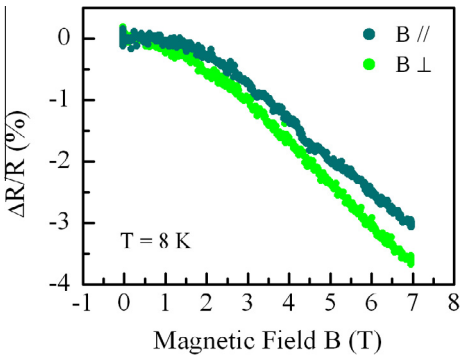

Fig. 7 – ΔR/R in four probe configuration of sample G (T_A = 900 °C) at T = 8 K. Dark green corresponds to magnetic field parallel to rGO plane, while light green indicates magnetic field perpendicular to rGO plane. (A color version of this figure can be viewed online.)

theoretically by several works [57–59], it has also experimentally been reported by a number of groups in different carbon systems [54,60–63]. As exposed above, rGO does not fully recover perfect graphene structure, but many defects remain in the final lattice after the reduction. These impurities/defects likely generate localized magnetic moments. Given the large number of these defects, it is therefore not surprising to observe the signal from magnetic impurities.

To clarify the origin of the magnetoresistance, we measured the dependence of the resistance on the magnetic field applied parallel to the rGO film plane. In Fig. 7 we present the $\Delta R/R$ for a sample G, T_A = 900 °C. The magnetoresistance measured at T = 8 K with the magnetic field B applied parallel to the GO film plane results to be of the same order of magnitude of the one measured with the field perpendicular to the sample plane. This lack of anisotropy excludes possible orbital origins, further corroborating our suspect on localized magnetic moments as source of the observed magnetoresistance.

Also, to exclude any contribution due to possible presence of Cr, which is used in the fabrication process of the electrical contacts, samples with Pd contacts were measured, finding similar results.

Very recently Qin and coworkers [54] showed non-saturating negative magnetoresistance in 1–10 layers of GO films reduced by annealing at 600 °C. They observed $\Delta R/R$ up to −2.5% at 5 K and 1 T, claiming that the origin is due to spin dependent scattering of defects. This value is consistent with our results, but they also report minor hysteresis loops in their magnetoresistance measurements which we did not observe. Sometimes hysteresis loops depend on the sweeping rate of the field; our measurements are performed at 200 Oe/s but also control tests have been done using different speeds as 50 Oe/s and 100 Oe/s, not showing any hysteresis.

4. Conclusions

We presented a protocol to produce distinct resistive states of rGO films by controlling the annealing temperature. We characterized the electrical and magnetic transport properties of rGO films at intermediate reduction degrees and in a wide temperature range (2–300 K). The temperature

dependence of the resistance fits $R = R_0\exp(T_0/T)^{1/3}$ for T well below the liquid nitrogen temperature, consistently with 2D Mott-VRH. At lower temperatures, a crossover to another regime likely occurs. High magnetoresistance values are measured at low temperature. These results extend the temperature and magnetic field range of previous works and evidence the interplay of different mechanisms of charge transport in rGO thin films. To discriminate and assess the validity of one mechanism for charge transport it is essential to observe a given $R(T)$ law in a sufficiently extended temperature range (more than one decade), and the limited temperature range of previous studies could be the reason of the diverse transport mechanisms claimed by the different authors. We also believe that a systematic study on single flake rGO could also shed light on the role of the transition from 2D to 3D of the electrical conduction, which is a possible cause of the reported deviations from the 2D hopping conduction model.

Acknowledgements

This work has been partially supported by European Community through the FET-Proactive Project "MoQuaS", contract N. 610449 and by the Italian Ministry for Research (MIUR) through the FIR Grant RBFR13YKWX. The research leading to these results has also received funding from the European Union Seventh Framework Programme under grant agreement n°604391 Graphene Flagship. The project UPGRADE acknowledges the financial support of the Future and Emerging Technologies (FET) programme within the Seventh Framework Programme for Research of the European Commission, under FET-Open grant number: 309056.

Appendix A. Supplementary data

Supplementary data associated with this article can be found, in the online version, at http://dx.doi.org/10.1016/j.carbon.2015.03.019.

REFERENCES

[1] Novoselov KS, Fal'Ko VI, Colombo L, Gellert PR, Schwab MG, Kim K. A roadmap for graphene. Nature 2012;490:192–200. http://dx.doi.org/10.1038/nature11458.

[2] Novoselov KS, Geim AK, Morozov SV, Jiang D, Zhang Y, Dubonos SV, et al. Electric field effect in atomically thin carbon films. Science 2004;306:666–9. http://dx.doi.org/10.1126/science.1102896.

[3] Brodie BC. On the atomic weight of graphite. Philos Trans R Soc Lond 1859;149:249–59.

[4] Treossi E, Melucci M, Liscio A, Gazzano M, Samorì P, Palermo V. High-contrast visualization of graphene oxide on dye-sensitized glass, quartz, and silicon by fluorescence quenching. J Am Chem Soc 2009;131(43):15576–7. http://dx.doi.org/10.1021/ja9055382.

[5] Melucci M, Durso M, Zambianchi M, Treossi E, Xia Z-Y, Manet I, et al. Graphene–organic hybrids as processable, tunable platforms for pH-dependent photoemission, obtained by a new modular approach. J Mater Chem 2012;22:18237–43. http://dx.doi.org/10.1039/C2JM33349J.

[6] Melucci M, Treossi E, Ortolani L, Giambastiani G, Morandi V, Klar P, et al. Facile covalent functionalization of graphene oxide using microwaves: bottom-up development of functional graphitic materials. J Mater Chem 2010;20:9052–60. http://dx.doi.org/10.1039/C0JM01242D.

[7] Liscio A, Veronese GP, Treossi E, Suriano F, Rossella F, Bellani V, et al. Charge transport in graphene–polythiophene blends as studied by Kelvin Probe Force Microscopy and transistor characterization. J Mater Chem 2011;21:2924–31. http://dx.doi.org/10.1039/C0JM02940H.

[8] Dikin DA, Stankovich S, Zimney EJ, Piner RD, Dommett GHB, Evmenenko G, et al. Preparation and characterization of graphene oxide paper. Nature 2007;448:457–60. http://dx.doi.org/10.1038/nature06016.

[9] Eda G, Fanchini G, Chhowalla M. Large-area ultrathin films of reduced graphene oxide as a transparent and flexible electronic material. Nat Nanotechnol 2008;3:270–4. http://dx.doi.org/10.1038/nnano.2008.83.

[10] Zhu Y, Murali S, Stoller MD, Ganesh KJ, Cai W, Ferreira PJ, et al. Carbon-based supercapacitors produced by activation of graphene. Science 2011;332:1537–41. http://dx.doi.org/10.1126/science.1200770.

[11] Liang H-W, Zhuang X, Brüller S, Feng X, Müllen K. Hierarchically porous carbons with optimized nitrogen doping as highly active electrocatalysts for oxygen reduction. Nat Commun 2014;5:4973. http://dx.doi.org/10.1038/ncomms5973.

[12] Han S, Wu D, Li S, Zhang F, Feng X. Porous graphene materials for advanced electrochemical energy storage and conversion devices. Adv Mater 2014;26(6):849–64. http://dx.doi.org/10.1002/adma.201303115.

[13] Xia ZY, Giambastiani G, Christodoulou C, Nardi MV, Koch N, Treossi E, et al. Synergic exfoliation of graphene with organic molecules and inorganic ions for the electrochemical production of flexible electrodes. ChemPlusChem 2014;79(3):439–46. http://dx.doi.org/10.1002/cplu.201300375.

[14] Yang S, Sun Y, Chen L, Hernandez Y, Feng X, Müllen K. Porous iron oxide ribbons grown on graphene for high-performance lithium storage. Sci Rep 2012;2:427. http://dx.doi.org/10.1038/srep00427.

[15] Wu Z-S, Yang S, Sun Y, Parvez K, Feng X, Müllen K. 3D nitrogen-doped graphene aerogel-supported Fe_3O_4 nanoparticles as efficient electrocatalysts for the oxygen reduction reaction. J Am Chem Soc 2012;134(22):9082–5. http://dx.doi.org/10.1021/ja3030565.

[16] Loh KP, Bao Q, Eda G, Chhowalla M. Graphene oxide as a chemically tunable platform for optical applications. Nat Chem 2010;2:1015–24. http://dx.doi.org/10.1038/nchem.907.

[17] Lu G, Ocola LE, Chen J. Reduced graphene oxide for room-temperature gas sensors. Nanotechnology 2009;20:445502. http://dx.doi.org/10.1088/0957-4484/20/44/445502.

[18] Borini S, White R, We D, Astley M, Haque S, Spigone E, et al. Ultrafast graphene oxide humidity sensors. ACS Nano 2013;7(12):11166–73. http://dx.doi.org/10.1021/nn404889b.

[19] Prezioso S, Perrozzi F, Giancaterini L, Cantalini C, Treossi E, Palermo V, et al. Graphene oxide as a practical solution to high sensitivity gas sensing. J Phys Chem C 2013;117(20):10683–90. http://dx.doi.org/10.1021/jp3085759.

[20] Erickson K, Erni R, Lee Z, Alem N, Gannett W, Zettl A. Determination of the local chemical structure of graphene oxide and reduced graphene oxide. Adv Mater 2010;22(40):4467–72. http://dx.doi.org/10.1002/adma.201000732.

[21] Dreyer DR, Park S, Bielawski CW, Ruoff RS. The chemistry of graphene oxide. Chem Soc Rev 2010;30:228–40. 0.1039/b917103g.

[22] He H, Klinowski J, Forster M, Lerf A. A new structural model for graphite oxide. Chem Phys Lett 1998;287(1):53–6. http://dx.doi.org/10.1016/S0009-2614(98)00144-4.
[23] Pei S, Cheng H-M. The reduction of graphene oxide. Carbon 2012;50:3210–28. http://dx.doi.org/10.1016/j.carbon.2011.11.010.
[24] Mattevi C, Eda G, Agnoli S, Miller S, Mkhoyan KA, Celik O, et al. Evolution of electrical, chemical, and structural properties of transparent and conducting chemically derived graphene thin films. Adv Funct Mater 2009;19(16):2577–83. http://dx.doi.org/10.1002/adfm.200900166.
[25] Perrozzi F, Prezioso S, Donarelli M, Bisti F, Marco PD, Santucci S, et al. Use of optical contrast to estimate the degree of reduction of graphene oxide. J Phys Chem C 2013;117(1):620–5. http://dx.doi.org/10.1021/jp3069738.
[26] Stankovich S, Dikin DA, Piner RD, Kohlhaas KA, Kleinhammes A, Jia Y, et al. Synthesis of graphene-based nanosheets via chemical reduction of exfoliated graphite oxide. Carbon 2007;45(7):1558–65. http://dx.doi.org/10.1016/j.carbon.2007.02.034.
[27] Mativetsky JM, Liscio A, Treossi E, Orgiu E, Zanelli A, Samorì P, et al. Graphene transistors via in situ voltage-induced reduction of graphene-oxide under ambient conditions. J Am Chem Soc 2011;133(36):14320–6. http://dx.doi.org/10.1021/ja202371h.
[28] Mativetsky JM, Treossi E, Orgiu E, Melucci M, Veronese GP, Samorì P, et al. Local current mapping and patterning of reduced graphene oxide. J Am Chem Soc 2010;132(40):14130–6. http://dx.doi.org/10.1021/ja104567f.
[29] Xia ZY, Pezzini S, Treossi E, Giambastiani G, Corticelli F, Morandi V, et al. The exfoliation of graphene in liquids by electrochemical, chemical, and sonication-assisted techniques: a nanoscale study. Adv Funct Mater 2013;23(37):4684–93. http://dx.doi.org/10.1002/adfm.201203686.
[30] Parvez K, Wu Z-S, Li R, Liu X, Graf R, Feng X, et al. Exfoliation of graphite into graphene in aqueous solutions of inorganic salts. J Am Chem Soc 2014;136(16):6083–91. http://dx.doi.org/10.1021/ja5017156.
[31] Gómez-Navarro C, Weitz RT, Bittner AM, Scolari M, Mews A, Burghard M, et al. Electronic transport properties of individual chemically reduced graphene oxide sheets. Nano Lett 2007;7(11):3499–503. http://dx.doi.org/10.1021/nl072090c.
[32] Kaiser AB, Gómez-Navarro C, Sundaram RS, Burghard M, Kern K. Electrical conduction mechanism in chemically derived graphene monolayers. Nano Lett 2009;9(9):1787–92. http://dx.doi.org/10.1021/nl803698b.
[33] Eda G, Mattevi C, Yamaguchi H, Kim H, Chhowalla M. Insulator to semimetal transition in graphene oxide. J Phys Chem C 2009;113(35):15768–71. http://dx.doi.org/10.1021/jp9051402.
[34] Venugopal G, Krishnamoorthy K, Mohan R, Kim S-J. An investigation of the electrical transport properties of graphene-oxide thin films. Mater Chem Phys 2012;132(1):29–33. http://dx.doi.org/10.1016/j.matchemphys.2011.10.040.
[35] Muchharla B, Narayanan TN, Balakrishnan K, Ajayan PM, Talapatra S. Temperature dependent electrical transport of disordered reduced graphene oxide. 2D Mater 2014;1(1):011008. http://dx.doi.org/10.1088/2053-1583/1/1/011008.
[36] Wang S-W, Lin HE, Lin H-D, Chen KY, Tu K-H, Chen CW, et al. Transport behavior and negative magnetoresistance in chemically reduced graphene oxide nanofilms. Nanotechnology 2011;22:335701. http://dx.doi.org/10.1088/0957-4484/22/33/335701.
[37] Joung D, Khondaker SI. Efros-Shklovskii variable-range hopping in reduced graphene oxide sheets of varying carbon sp^2 fraction. Phys Rev B 2012;86:235423. http://dx.doi.org/10.1103/PhysRevB.86.235423.
[38] Zhou Y-B, Han B-H, Liao Z-M, Wu H-C, Yu D-P. From positive to negative magnetoresistance in graphene with increasing disorder. Appl Phys Lett 2011;98:222502. http://dx.doi.org/10.1063/1.3595681.
[39] Russier J, Treossi E, Scarsi A, Perrozzi F, Dumortier H, Ottaviano L, et al. Evidencing the mask effect of graphene oxide: a comparative study on primary human and murine phagocytic cells. Nanoscale 2013;5:11234. http://dx.doi.org/10.1039/c3nr03543c.
[40] Becerril HA, Mao J, Liu Z, Stoltenberg RM, Bao Z, Chen Y. Evaluation of solution-processed reduced graphene oxide films as transparent conductors. ACS Nano 2008;2(3):463–70. http://dx.doi.org/10.1021/nn700375n.
[41] Pimenta MA, Dresselhaus G, Dresselhaus MS, Cançado LG, Jorioa A, Saito R. Studying disorder in graphite-based systems by Raman spectroscopy. Phys Chem Chem Phys 2007;9:1276–90. http://dx.doi.org/10.1039/B613962K.
[42] Ferrari AC, Robertson J. Interpretation of Raman spectra of disordered and amorphous carbon. Phys Rev B 2000;61:14095. http://dx.doi.org/10.1103/PhysRevB.61.14095.
[43] Eigler S, Dotzer C, Hirsch A. Visualization of defect densities in reduced graphene oxide. Carbon 2012;50(10):3666–73. http://dx.doi.org/10.1016/j.carbon.2012.03.039.
[44] Punckt C, Muckel F, Wolff S, Aksay IA, Chavarin CA, Bacher G, et al. The effect of degree of reduction on the electrical properties of functionalized graphene sheets. Appl Phys Lett 2013;102:023114. http://dx.doi.org/10.1063/1.4775582.
[45] Sahoo S, Khurana G, Barik SK, Dussan S, Barrionuevo D, Katiyar RS. In situ Raman studies of electrically reduced graphene oxide and its field-emission properties. J Phys Chem C 2013;117:5485–91. 10.1021/jp400573w.
[46] Ramesha GK, Sampath S. Electrochemical reduction of oriented graphene oxide films: an in situ Raman spectroelectrochemical study. J Phys Chem C 2009;113(19):7985–9. http://dx.doi.org/10.1021/jp811377n.
[47] Tung VC, Allen MJ, Yang Y, Kaner RB. High-throughput solution processing of large-scale graphene. Nat Nanotechnol 2009;4:25–9. http://dx.doi.org/10.1038/nnano.2008.329.
[48] Tuinstra F, Koenig JL. Raman spectrum of graphite. J Chem Phys 1970;53:1126. http://dx.doi.org/10.1063/1.1674108.
[49] Yang D, Velamakanni A, Bozoklu G, Park S, Stoller M, Piner RD, et al. Chemical analysis of graphene oxide films after heat and chemical treatments by X-ray photoelectron and Micro-Raman spectroscopy. Carbon 2009;47:145–52. http://dx.doi.org/10.1016/j.carbon.2008.09.045.
[50] Han F, Yang Shuming, Jing Weixuan, Jiang Kyle, Jiang Zhuangde, Liu Huan, et al. A highly efficient synthetic process of graphene films with tunable optical properties. Appl Surf Sci 2014;314:71–7. http://dx.doi.org/10.1016/j.apsusc.2014.05.222.
[51] Mott NF, Davis A. Electronic processes in non-crystalline materials. England: Oxford University Press; 1971.
[52] Gómez-Navarro C, Meyer JC, Sundaram RS, Chuvilin A, Kurasch S, Burghard M, et al. Atomic structure of reduced graphene oxide. Nano Lett 2010;10(4):1144–8. http://dx.doi.org/10.1021/nl9031617.
[53] Jung I, Dikin DA, Piner RD, Ruoff RS. Tunable electrical conductivity of individual graphene oxide sheets reduced at "low" temperatures. Nano Lett 2008;8(12):4283–7. http://dx.doi.org/10.1021/nl8019938.
[54] Qin S, Guo Xitao, Cao Yanqiang, Ni Zhenhua, Xu Q. Strong ferromagnetism of reduced graphene oxide. Carbon 2014;78:559–65. http://dx.doi.org/10.1016/j.carbon.2014.07.039.

[55] Bobbert PA, Nguyen TD, Oost FWaV, Koopmans B, Wohlgenannt M. Bipolaron mechanism for organic magnetoresistance. Phys Rev Lett 2007;99:216801. http://dx.doi.org/10.1103/PhysRevLett. 99.216801.
[56] Alexandrov AS, Dediu VA, Kabanov VV. Hopping magnetotransport via nonzero orbital momentum states and organic magnetoresistance. Phys Rev Lett 2012;108:186601. http://dx.doi.org/10.1103/PhysRevLett. 108.186601.
[57] Palacios JJ, Fernández-Rossier J, Brey L. Vacancy-induced magnetism in graphene and graphene ribbons. Phys Rev B 2008;77:195428. http://dx.doi.org/10.1103/PhysRevB.77.195428.
[58] Uchoa B, Kotov VN, Peres NMR, Neto AHC. Localized magnetic states in graphene. Phys Rev Lett 2008;101:026805. http://dx.doi.org/10.1103/PhysRevLett. 101.026805.
[59] Krasheninnikov AV, Lehtinen PO, Foster AS, Pyykkö P, Nieminen RM. Embedding transition-metal atoms in graphene: structure, bonding, and magnetism. Phys Rev Lett 2009;102:126807. http://dx.doi.org/10.1103/PhysRevLett. 102.126807.
[60] Ugeda MM, Brihuega I, Guinea F, Gomez-Rodrıguez JM. Missing atom as a source of carbon magnetism. Phys Rev Lett 2010;104:096804. http://dx.doi.org/10.1103/PhysRevLett. 104.096804.
[61] Feng Q, Tang N, Liu F, Cao Q, Zheng W, Ren W, et al. Obtaining high localized spin magnetic moments by fluorination of reduced graphene oxide. ACS Nano 2013;7(8):6729–34. http://dx.doi.org/10.1021/nn4027905.
[62] Candini A, Alvino C, Wernsdorfer W, Affronte M. Hysteresis loops of magnetoconductance in graphene devices. Phys Rev B 2011;83:121401. http://dx.doi.org/10.1103/PhysRevB.83.121401.
[63] Khurana G, Kumar N, Kotnala RK, Nautiyal T, Katiyar RS. Temperature tuned defect induced magnetism in reduced graphene oxide. Nanoscale 2013;5:3346–51. http://dx.doi.org/10.1039/C3NR34291C.